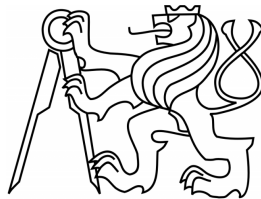


CZECH TECHNICAL UNIVERSITY IN
PRAGUE

FACULTY OF NUCLEAR SCIENCES AND PHYSICAL
ENGINEERING

Department of Physics



RESEARCH PROJECT

**Electroproduction of Kaons on
Protons in Regge-plus-resonance
Approach**

Dalibor Skoupil

2011

Supervisor: RNDr. Petr Bydžovský, CSc.

Acknowledgement

I would like to thank my supervisor RNDr. Petr Bydžovský, Csc. for his willingness, for his continuous support during writing of this thesis, for the amount of information he gave me about this topic and for many useful hints, which helped me.

In addition, I would like to thank all the people in my surroundings for their support and assistance.

Contents

1	Preface	1
2	Introduction	3
2.1	Historical Background	3
2.2	Underlying physics	4
2.3	Various Approaches to the Strangeness	
	Electromagnetic Production	6
3	Review of the Isobar Model	9
3.1	Properties of the Isobar Model	11
4	The Regge Model	15
4.1	Regge trajectories	17
4.2	Regge propagators	18
4.3	Restoring gauge invariance	20
5	The Regge-plus-resonance Model	21
5.1	Inclusion of resonance contributions	21
6	Program for the RPR Model	25
6.1	Discussion about the Outcomes	28
7	Conclusion	31
A	Isobar Model Formalism	33
A.1	CGLN Amplitudes	33

CONTENTS

Chapter 1

Preface

The aim of this work is to deal with the production of pseudoscalar mesons on nucleons induced by electrons at energy of few GeV. This process is suitable for investigating properties of baryons and their resonances. The tool for studying this process is models based on the tree-level perturbation theory of the effective hadronic Lagrangian. Free parameters in the Lagrangian are determined by fitting on the experimental data.

It is believed, that the particle electromagnetic production will bring some deeper insight into the structure of hadrons. Therefore, it is an important and very promising field of study. Moreover, thanks to the particle production, one can study the resonance properties.

Although there are many ways to study the particle production, the most challenging process is the kaon photo- and electroproduction. Since the electromagnetic part of the process is well understood, the kaon production is relatively easy to describe.

There are several ways how to describe these production processes, but the most promising approaches are the isobar models and Regge-plus-resonance (RPR) model. Especially to the latter, we will pay special attention in this thesis.

The main task of the research project is to compose a program for the RPR model.

In this work, the second chapter is related to a brief introduction to the problematics (there is shown the historical overview and some approaches are sketched). Chapters three and four serve to describe the fundamental properties of the isobar model, Regge model and the hybrid RPR model. After that, the program for the the RPR model is discussed and some outcomes are shown.

Chapter 2

Introduction

2.1 Historical Background

The beginning of both theoretical and experimental study of kaon photo- and electroproduction was given in the year 1957, when both Caltech [10] and Cornell [19] laboratories released the $p(\gamma, K^+)\Lambda$ cross-section data obtained at their electron synchrotrons. There were a plenty of data collected on the kaon photoproduction (Caltech, Cornell, etc. [6]) but only a few experiments were realized on the electroproduction (DESY, Cambridge [6]).

The modeling of kaon photoproduction processes started by the pioneering work of Kuo [15], later followed by Thom [23]. The few datapoints reported in these pioneering publications were of a limited accuracy, and only the kinematical region very close to threshold could be probed due to the limited electron energies available at that time.

Further experiments were performed in the 1970s and 1980s, not only in the USA but also at facilities in Bonn [1] and Tokyo [11]. After that, one had to wait until the year 1998, when the SAPHIR collaboration, operating at the Bonn ELSA facility, released the first high precision data for all three reaction channels on the proton target $p(\gamma, K^+)Y$, with $Y = \Lambda, \Sigma^0$,

and $p(\gamma, K^0)\Sigma^+$ over the photon laboratory energy range from threshold up to 2 GeV [22]. The SAPHIR data clearly triggered revived interest in the theoretical community in the search for missing resonances.

The study of meson photoproduction at intermediate energy ($E_\gamma^{lab} \geq 4$ GeV) becomes now experimentally accessible in a systematic way with the high-duty cycle electron facilities like TJNAF. In particular, the combination of the large acceptance detector CLAS and the high intensity beam of TJNAF, makes possible the study of meson photo- and electroproduction reactions at large angle and opens up an unexplored field [13].

Over the past years, the amount of data of the process (γ^*, K^+) has been substantially extended with a high precision data from the CLAS (2005, 2007 and 2010) [18, 2, 3], SAPHIR (2003) [12], LEPS (2003, 2006 and 2007) [24, 21] and GRAAL (2007) [17] collaborations. In addition, the SAPHIR collaboration has also provided a new analysis of the $p(\gamma, K^0)\Sigma^+$ channel [16].

2.2 Underlying physics

As it was written in the previous section, the investigation of strangeness production from a proton, using real or virtual photons, started in the late fifties, but a comprehensive description of the underlying mechanism is still not available. This uncomfortable situation, compared for example to pion production, which is dominated basically by one nucleonic resonance, might be attributed to the more complex role played by the strange quark versus that arised by u and d quarks. The introduction of this additional degree of freedom leads to the fact that, even close to the threshold, a rather ample number of hyperonic and nucleonic resonances may intercede the process.

The following reactions are being or will be studied in the near future:

$$\gamma + p \longrightarrow K^+ + \Lambda, \quad (2.1)$$

$$\gamma + p \longrightarrow K^+ + \Sigma^0, \quad (2.2)$$

$$\gamma + p \longrightarrow K^0 + \Sigma^+, \quad (2.3)$$

Reaction (2.1) is the one most studied, both experimentally and theoretically, including polarization observables measurements; although, a large part of the existing data base suffers from inconsistencies within the reported accuracies. There are less extensive investigations of the reaction (2.2). The third process has received very little consideration, probably because of experimental difficulties in identifying the final state properties.

The high-duty electron and photon facilities like CEBAF, MAMI, ELSA, SPring-8, etc. also allow envisioning high quality electroproduction data for the elementary reactions

$$e + p \longrightarrow e' + K^+ + \Lambda \quad (2.4)$$

$$e + p \longrightarrow e' + K^+ + \Sigma^0 \quad (2.5)$$

$$e + p \longrightarrow e' + K^0 + \Sigma^+ \quad (2.6)$$

In these processes, the virtual photon polarisation has besides the transverse component also a longitudinal part and offers the possibility of varying independently the energy and momentum transfers. In this respect, the electrons are a finer probe for the strangeness domain [9].

Although each of the above introduced reactions is interesting by itself, a necessary step by step investigation requires first the understanding of the

photoproduction reactions. The electroproduction processes can be formally reduced to an investigation of the binary processes of the photoproduction by virtual photons since the electromagnetic coupling constant is small enough to justify the one-photon approximation. An extension to the electroproduction processes constitutes the next stage. Subsequently, we can take benefit of the much cleaner electromagnetic probes, compared to hadronic ones, to study the strangeness in composite hadronic systems, especially in the hypernuclei physics.

2.3 Various Approaches to the Strangeness

Electromagnetic Production

In general, the theoretical approaches to electromagnetic strangeness production fall into two categories. In parton-based models, the quark-gluon structure of the interacting hadrons is explicitly tied in with the reaction dynamics. In contrast, hadrodynamical approaches consider the interacting hadrons themselves as the basic degrees of freedom of the effective field theory. In such an approach, the hadrons are treated as effective particles with specific properties.

Except at very high energies, where QCD can be solved perturbatively, quarks and gluons do not represent the optimum building blocks in hadron reaction models. More appropriate degrees of freedom in the nonperturbative regime are the bound states of constituent quarks, i.e. mesons and baryons. Since we are not able to fully determine the properties of these objects by the fundamental field theories, the hadrons are referred to as effective degrees of freedom. Which effective building blocks to use depends on the energies one aims to describe. Near the $p(\gamma, K^+)\Lambda$ threshold there are obvious structures in the cross sections, reflecting the production of in-

dividual N^* and/or Δ^* states. A logical strategy to model these states is to employ hadrons in their entirety as effective degrees of freedom.

There are several approaches to the treatment of the photoproduction process. Among them, the isobar models based on the effective Lagrangian description considering only the hadronic degrees of freedom are suitable for their further use in the more complex calculations. The other approaches are suitable either for higher energies ($E_\gamma^{lab} > 4 \text{ GeV}$) - the Regge model, or to the threshold region - the Chiral Perturbation Theory. Quark models are too complicated for their further use in hypernuclear calculations. Another approach, aimed at the forward-angle production, is the hybrid Regge-plus-resonance model in which the background part of amplitude is generated by the t -channel Regge-trajectory exchange and the resonant behaviour is shaped by the s -channel resonances like in an isobar model.

Chapter 3

Review of the Isobar Model

In this chapter I will review the basics of isobar model. In my previous work - bachelor thesis, I have studied this model. Therefore, some more information about the isobar model is available in this work [20].

Let us introduce the main thoughts of the isobar model. The starting point in modeling the $p(\gamma, K^+)\Lambda$ processes is a description in terms of hadronic degrees of freedom. This means that in these models the reaction amplitude is derived from an effective hadronic Lagrangian using the Feynman diagrammatic technique in the tree-level approximation (these are the diagrams with the smallest possible number of interaction vertices). The Feynman diagrams contribute to the background (or nonresonant) and the resonant part of the amplitude. The diagrams containing the intermediate nucleon excitations (or resonances) are referred to as the resonant diagrams, as they can produce peaks in the cross section.

As can be seen from Fig. (3.1), the various types of tree-level diagrams can be classified in several ways. The left column collects Born terms, which have a ground-state hadron in the intermediate state (one can further distinguish between s -, t -, u -channel contributions). The t - and u -channel diagrams and the s -channel Born term are background contributions, as

energy-momentum conservation prevents their poles from being reached in physical plane. Only the s -channel non-Born term (the red diagram involving an excited state) produces resonant structures in the observables.

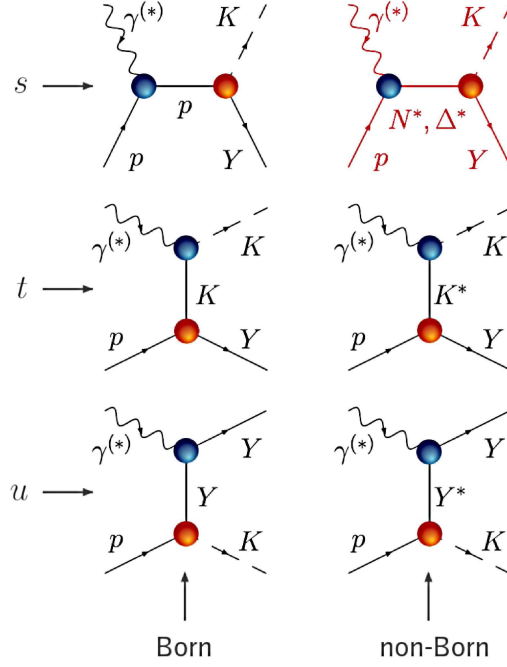


Figure 3.1: Tree-level contributions to the $p(\gamma, K)Y$ amplitude ($Y = \Lambda, \Sigma^{0,+}$). The Δ^* states can only be produced in the $K\Sigma$ channels due to isospin conservation. The Mandelstam variables s , t and u are defined by $s = (p_p + p_\gamma)^2$, $t = (p_\gamma - p_K)^2$ and $u = (p_p - p_K)^2$, respectively, where $p_\gamma = (E_\gamma, \vec{p}_\gamma)$, p_p , p_K , and p_Y are the four-vectors of the asymptotic particles playing a role in this process.

To summarize, this kind of description (i.e. the tree-level effective-field approach) is commonly referred to as the isobar model. It is the near-threshold and resonant kinematic region involving photon-laboratory energies $E_\gamma^{lab} = 0.91 - 2.5$ GeV, where this model is of particular interest [4].

Despite the long history and the large amount of both experimental and theoretical efforts, a complete understanding of the $p(\gamma, K^+)\Lambda$ reaction mechanism still remains problematic. Firstly, there is a lot of nucleon

and hyperon resonances that contribute to the process, which results in a great number of versions of the isobar model [4] (for instance, we can mention the Kaon-MAID or Saclay-Lyon model [9]). Secondly, the Born terms in their own predict the $p(\gamma, K^+)\Lambda$ cross sections which are a few times the measured ones [14].

Since 1990, three major models, based on isobaric approaches, have been published. The first one by Adelseck-Saghai focuses on the reaction (2.1) for $E_\gamma^{lab} \leq 1.5$ GeV. The second one, by Williams, Ji, and Cotanch investigates all the reactions (2.1)-(2.6) mentioned in previous chapter except the $p(\gamma, K^0)\Sigma^+$ channel, and extends the energy range to $E_\gamma^{lab} \leq 2.1$ GeV. Finally, the third model, by Mart, Bennhold, and Hyde-Wright, is dedicated to the $K\Sigma$ photoproduction channels with a special emphasis on the charged Σ production in the same energy range as the model by Williams et al. [9].

3.1 Properties of the Isobar Model

Although built upon the same set of formal principles, effective-Lagrangian models face a number of challenges unknown to the fundamental field theories.

Form Factors

Hadrons are not pointlike particles, but have an internal structure. As a consequence, they manifest themselves differently according to the resolution at which they are probed. This can be formally expressed by modifying the effective coupling constants with appropriate form factors.

The strong or hadronic form factors are the running coupling constants at the hadronic vertices. The form most commonly assumed in literature is

a dipole [6]

$$F_x = \frac{\Lambda_h^4}{\Lambda_h^4 + (x - m_h^2)^2},$$

with x the squared four-momentum of the intermediate hadron h , and m_h its mass. The cutoff mass Λ_h determines the high-energy (and therefore short-range) behaviour of the interaction. It can be used as a free parameter when optimizing the model parameters against the data. A single cutoff value Λ_{res} is usually assumed for all resonant diagrams, whereas for background diagrams another value Λ_{bg} is used. It is well-known that introducing the hadronic form factors violates the gauge invariance at the level of the Born diagrams. Additional contact term (i.e. diagram which do not contain any pole) is then required to restore this fundamental symmetry [14].

The electromagnetic form factors depend on $Q^2 = -k^2$, with k the incoming photon momentum. They are normalized so that they reduce to either 0 or 1 in the real-photon point [6].

Unitarity

Since the unitarity requirement is linked to the conservation of probability, it is automatically fulfilled for the fundamental interactions. However, effective field theories are not necessarily unitary by construction. When restricting ourselves to the tree-level diagrams, there is need to plug the decay widths of the various resonances in by hand. This can be reached through the substitution

$$s - m_R^2 \longrightarrow s - m_R^2 + im_R\Gamma_R$$

in the propagator denominators, with m_R and Γ_R the mass and the width of the propagating state ($R = N^*, \Delta^*$), respectively. This procedure is applied solely to the resonant diagrams, where the exchanged particle can be on its mass-shell in the physical region of the process.

Higher-order Corrections

It is obvious that the isobar approach, such as any other model, has its limitations. Apparently, by truncating the amplitude at tree level, higher-order mechanisms like channel couplings and final-state interactions are excluded from the reaction mechanism.

The importance of this issue becomes clear when realizing e. g. that the $\pi + N \rightarrow \pi + N$ cross sections are many times larger than the $\gamma + p \rightarrow K + Y$ ones. In other words, contributions from higher-order processes, such as the one shown in Fig. (3.2), are not necessarily less important than the tree-level diagrams.

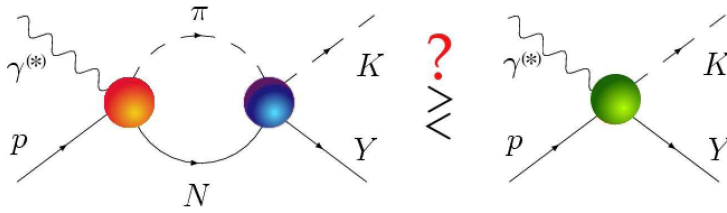


Figure 3.2: A typical higher-order contribution to $p(\gamma, K)Y$ (on the left side) compared to the direct process (right).

Although Chiang *et al.* [5] have shown that the contributions of the intermediate πN channel to the $p(\gamma, K^+)\Lambda$ cross sections are of the order of 20 %, the success of the isobar approach in describing even the most recent data demonstrates that lowest-order diagrams are well able to imitate certain higher-order effects.

However, when comparing the coupling constants found in the context of a tree-level model to calculated or measured values, one has to be cautious.

In this work, channel-coupling effects are not taken into account.

Chapter 4

The Regge Model

A major drawback of the isobar model introduced in previous chapter is its limited scope in energy. Specifically, isobar approaches fail to meet a necessary condition for unitarity, known as the Froissart bound, which constitutes an upper limit on the high-energy behaviour of the cross sections. A realistic total scattering cross section is allowed to increase with energy no faster than $\log^2\left(\frac{s}{s_0}\right)$. In an isobar framework, however, the background contribution rises as a positive power of s . Up to a certain energy, this rise can be compensated by destructive interferences with other resonant and nonresonant diagrams. For center-of-mass energies higher than a few GeV, where adding individual resonances no longer makes sense, unphysical behaviour develops [6].

A solution is provided by a high-energy framework introduced by Tullio Regge in the year 1959. Regge's starting point was to consider the partial-wave amplitudes as a function of a complex angular momentum variable. Interestingly, poles of the amplitude were found to correspond to resonant states, which could be sorted into several families. The members of such a family, the Regge trajectory, turned out to share identical internal quantum numbers, such as strangeness or isospin, while having different total spins.

Regge theory rests upon the proposition that, at energies where individual resonances can no longer be distinguished, the reaction dynamics are governed by the exchange of entire Regge trajectories rather than of single particles. The high-energy Regge framework employed here applies to the so-called "Regge limit" of extreme forward (in the case of t -channel exchange) or backward (for u -channel exchange) scattering angles, corresponding to small $|t|$ or $|u|$, respectively. In this work, we focus on the forward-angle kinematical region which, for electromagnetic KY production, implies the exchange of kaonic trajectories in the t -channel (in the u -channel, the Y^* trajectories are exchanged). The diagrams contributing to the high-energy, forward-angle $K^+\Lambda$ photoproduction amplitude are shown in Fig. (4.1). We refer to them as background terms, because none of them passes through a pole in the physical plane of the $p(\gamma, K^+)\Lambda$ process.

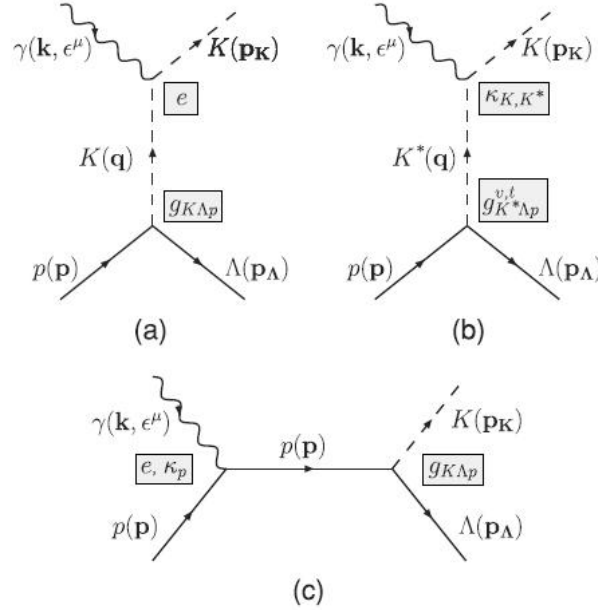


Figure 4.1: Feynman graphs contributing to the $p(\gamma, K^+)\Lambda$ amplitude for $E_\gamma^{lab} \geq 4 \text{ GeV}$ and at forward angles: exchange of (a) K and (b) K^* trajectories. The electric part of the s -channel Born term, diagram (c), is added to restore gauge invariance.

There are two reasons why we have chosen not to treat the u -channel reggeization. Firstly, the high-energy data in the backward-angle regime are scarce. And the second, more fundamental, reason involves the fact that the lightest hyperon, the Λ is significantly heavier than a K meson. As a consequence, the u -channel poles are removed much further from the backward-angle kinematical regime than the t -channel poles are from the forward-angle region. Therefore, for u -channel reggeization, the procedure of requiring the Regge propagator to reduce to the Feynman one at the closest crossed-channel pole cannot be guaranteed to lead to good results.

4.1 Regge trajectories

Empirically, it is observed that the meson trajectories $\alpha_X(t)$

$$\alpha_X(t) = \alpha_{X,0} + \alpha'_X(t - m_X^2),$$

with m_X the mass and $\alpha_{X,0}$ the spin of the trajectory's lightest member (or "first materialization") X , relating the spins and squared masses of the hadronic trajectory members are linear to a very good approximation. Figure (4.2) illustrates that statement by showing the J versus m^2 plots (also known as Chew-Frautschi plots) for the trajectories with $K(494)$ and $K^*(892)$ as their lightest members. There are only two trajectories taken into account when modeling the background of the $p(\gamma, K^+)\Lambda$ process.

There are just three parameters needed to quantify them. For $K(494)$ it is the $g_{K^+\Lambda p}$ coupling constant. For the $K^*(892)$ trajectory one needs to constrain the vector $g_{K^+\Lambda p}^v$ and tensor $g_{K^+\Lambda p}^t$ couplings [7].

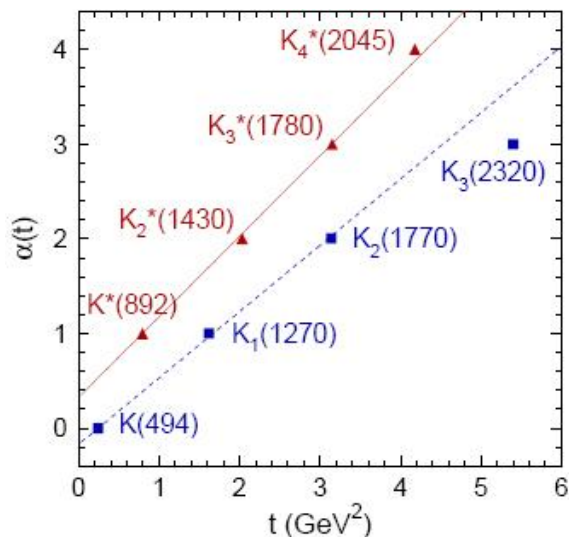


Figure 4.2: Chew-Frautschi plots for the $K(494)$ and $K^*(892)$ trajectories. The meson masses are from the Particle Data Group.

4.2 Regge propagators

An efficient way to model trajectory exchanges involves embedding the Regge formalism into a tree-level effective-field model. The amplitude for t -channel exchange of a linear kaon trajectory $\alpha(t)$ can be obtained from the standard Feynman amplitude by replacing the usual pole-like Feynman propagator of a single particle with a Regge one

$$\frac{1}{t - m_X^2} \longrightarrow \mathcal{P}_{Regge}^X[s, \alpha_X(t)],$$

while keeping the vertex structure given by the Feynman diagrams which correspond to the first materialization of the trajectory.

The Regge amplitude can then be written as

$$\mathcal{M}_{Regge}^X(s, t) = \mathcal{P}_{Regge}^X[s, \alpha_X(t)] \times \beta_X(s, t),$$

with $\beta_X(s, t)$ the residue of the original Feynman amplitude, calculated from the interaction Lagrangians at the $\gamma^{(*)}KX$ and pXY vertices.

In our treatment of $K^+\Lambda$ and $K^+\Sigma^0$ photoproduction, we identify the $K(494)$ and $K^*(892)$ trajectories as the dominant contributions to the high-energy amplitudes. The corresponding propagators assume the following form [8]

$$\mathcal{P}_{Regge}^{K(494)}(s, t) = \left(\frac{s}{s_0}\right)^{\alpha_K(t)} \frac{1}{\sin(\pi\alpha_K(t)) \Gamma(1 + \alpha_K(t))} \left\{ \begin{matrix} 1 \\ e^{-i\pi\alpha_K(t)} \end{matrix} \right\},$$

$$\mathcal{P}_{Regge}^{K^*(892)}(s, t) = \left(\frac{s}{s_0}\right)^{\alpha_{K^*}(t)-1} \frac{1}{\sin(\pi\alpha_{K^*}(t)) \Gamma(1 + \alpha_{K^*}(t))} \left\{ \begin{matrix} 1 \\ e^{-i\pi\alpha_{K^*}(t)} \end{matrix} \right\},$$

with trajectory equations given by [8]

$$\alpha_K(t) = 0.70(t - m_K^2),$$

$$\alpha_{K^*}(t) = 1 + 0.85(t - m_{K^*}^2).$$

The phase of these propagators can be either constant (1) or rotating ($e^{-i\pi\alpha(t)}$), depending on the relative sign between the residues of the individual signature parts.

As can be seen from the definition of the Regge propagators, they have poles at nonnegative integer values of $\alpha(t)$, corresponding to the zeroes of $\sin(\pi\alpha(t))$ which are not compensated by the poles of $\Gamma(1 + \alpha(t))$. Thence comes the interpretation that the Regge propagator effectively incorporates the exchange of all members of the $\alpha(t)$ trajectory. However, in the physical region of the processes under study (with $t < 0$), these poles cannot be reached.

Whether or not a trajectory should be treated as degenerate depends less on the trajectory equations themselves than on the process under study. Non-degenerate trajectories give rise to dips in the differential cross section because they exhibit so-called wrong-signature zeroes (these are zeroes of the Regge propagator corresponding to poles of the gamma function which are

not removed by the sine function in the denominator). Vice versa, a smooth, structureless cross section points to degenerate trajectories. Because no obvious structure is present in the $p(\gamma, K^+)\Lambda$ cross-section data for $E_\gamma^{lab} \geq 4$ GeV, both the K and K^* trajectories are assumed to be degenerate.

However, it can seem strange that a certain trajectory may need to be treated as degenerate in one hadronic process, but as non-degenerate in another. This apparent inconsistency is easily explained when realizing that the determining factors for degeneracy are the residues of the positive and negative-signature amplitudes, which obviously depend on the specific initial and final state [7].

4.3 Restoring gauge invariance

An essential property of any theory dealing with electromagnetic interactions is gauge invariance, related by the Noether theorem to the principle of charge conservation.

It is argued that, apart from the $K^+(494)$ and $K^{*+}(892)$ trajectory exchanges, the Regge amplitude for K^+ photoproduction should also include a contribution from the electric part of the s -channel Born term (as a counter term to the exchange of the lowest pole in the K^+ trajectory), as visualised in Fig. (4.1) [8]. This can be accomplished through the recipe

$$\mathcal{M}_{Regge}(\gamma p \rightarrow K^+ \Lambda) = \mathcal{M}_{Regge}^{K^+(494)} + M_{Regge}^{K^{*+}(892)} + \mathcal{M}_{Feyn}^{p,elec} \times \mathcal{P}_{Regge}^{K^+} \times (t - m_{K^+}^2).$$

This procedure is necessary because of the gauge-breaking nature of the K^+ -exchange diagram. In a typical effective-Lagrangian framework the Born terms $\mathcal{M}_{Feyn}^{p,K,Y}$ in the s -, t - and u -channels do not individually obey gauge invariance, but their sum does. It can be shown [6], that implementing this gauge-invariance restoration procedure leads to an improved description of the high-energy $p(\gamma, K^+)\Lambda$ differential cross section at $|t| \rightarrow 0$.

Chapter 5

The Regge-plus-resonance

Model

As it was written in the previous chapter, the Regge theory is a high-energy tool by construction. The experimental meson production cross sections are observed to exhibit Regge behaviour for photon energies as low as 4 GeV. Even in the resonance region, the order of magnitude of the forward-angle pion and kaon electromagnetic production observables is remarkably well reproduced in the Regge model [8].

5.1 Inclusion of resonance contributions

Nonetheless, it is evident that a pure background description such as the Regge-pole model cannot be expected to describe the reaction at energies in the resonance region. The near-threshold cross sections exhibit structures, such as peaks at certain energies and sudden variations in the angular distributions, which may reflect the presence of individual resonances. These are incorporated into the Regge-plus-resonance (RPR) model by supplementing the reggeized background with a small number of resonant s -channel

diagrams. For the latter, standard Feynman propagators are assumed, in which, as in the isobar approach, the resonances' finite lifetimes are taken into account through the substitution [8]

$$s - m_R^2 \longrightarrow s - m_R^2 + im_R\Gamma_R,$$

in the propagator denominators, with the m_R and Γ_R the mass and width of the propagating state ($R = N^*, \Delta^*$).

In conventional isobar models, the resonance contributions increase with energy. However, for the RPR approach to be meaningful the resonance amplitudes should vanish at high values of E_γ^{lab} . This is accomplished by including a Gaussian hadronic form factor $F(s)$ (on the contrary to the dipole form factor used in the isobar approach) at the strong KYR vertices

$$F(s) = \exp \left\{ -\frac{(s - m_R^2)^2}{\Lambda_{res}^4} \right\}. \quad (5.1)$$

A single cutoff mass Λ_{res} is assumed for all resonances. Along with the resonance couplings, Λ_{res} is used as a free parameter when optimizing the model against the resonance-region data. The motivation for introducing Gaussian form factors instead of dipole form factors is that they fall off much more sharply with energy than dipoles [6], as can be seen from Fig. (5.1).

By construction, the RPR amplitude is valid over the entire energy region described by the isobar and Regge models, i.e. from threshold up to about 20 GeV. In the high-energy regime (E_γ^{lab}), all resonant contributions vanish by construction, so that only the Regge part of the amplitude remains.

The RPR amplitude in its entirety involves t -channel exchanges of kaonic trajectories as well as s -channel Feynman diagrams corresponding to individual baryon resonances. In Fig. (5.2), the RPR amplitude is shown.

The greatest benefit of the RPR strategy, apart from its wide energy range, is the elegant description of the non-resonant part of the reaction

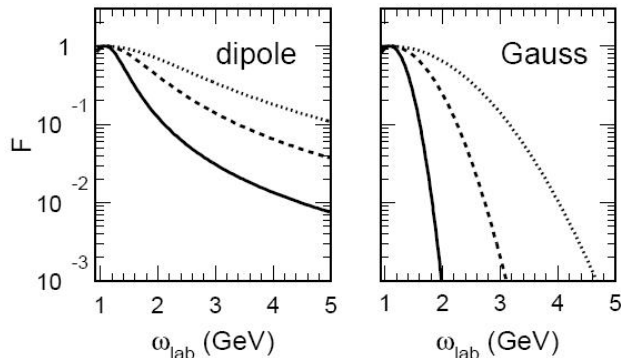


Figure 5.1: Dipole and Gaussian form factors as a function of the photon energy in the lab frame E_γ^{lab} for a resonance with mass $m_{N^*} = 1710$ MeV. The full, dashed and dotted curves correspond to cutoffs $\Lambda_{res} = 800, 1200$ and 1600 MeV, respectively.

amplitude. In standard isobar model, the determination of the background requires a significantly larger number of parameters. A Regge-inspired model is limited to t - or u -channel exchanges, with only a small number of trajectories required in either case. In the Regge model, there is only one additional uncertainty, namely the choice between constant or rotating phase.

One point which may obscure the procedure of constructing the RPR amplitude is a double counting, caused, according to the duality principle, by adding a small number of individual resonances onto the Regge background. As the $p(\gamma, K)Y$ processes are largely dominated by background contributions, the few s -channel terms may be considered as relatively subordinate corrections, and therefore the double counting is not expected to be a significant issue [6].

$$\mathcal{M}_{RPR} = \sum_{\mathcal{K}} \left(\begin{array}{c} \begin{array}{c} \gamma \text{ (wavy)} \nearrow \\ \text{red vertex} \\ \downarrow \alpha_{\mathcal{K}}(t) \\ \text{blue vertex} \\ p \nearrow \quad Y \searrow \\ (p\mathcal{K}Y) \end{array} \\ \text{Regge} \end{array} \right) + \sum_R \left(\begin{array}{c} \begin{array}{c} \gamma \text{ (wavy)} \nearrow \\ \text{red vertex} \\ \xrightarrow{R} \text{blue vertex} \\ p \nearrow \quad Y \searrow \\ (\gamma pR) \quad (RKY) \end{array} \\ \text{Feyn} \end{array} \right)$$

Figure 5.2: General forward-angle RPR amplitude for the $p(\gamma, K)Y$ process.

Chapter 6

Program for the RPR Model

As was discussed in the previous chapters, the Regge-plus-Resonance (RPR) is a hybrid model, which consists of two parts - the first part is the Regge model, which describes only background contributions, and the second part is the isobar model, which depicts the resonant kinematic region. The illustration of how these models work on their energy regions is shown in Figs. (6.2) and (6.3).

In the past few years, the programs (either for Regge model or for isobar model) were created by my supervisor Petr Bydžovský. These programs work reliably and give results in perfect correspondence with works of other authors.

The main task of this work was to put these well-working programs together. As the program for isobar model has better organized and more synoptic input, we decided to take this program as the cornerstone of the new program for the RPR model. Since the Regge model consists only of nonresonant (background) diagrams, it cannot be expected to account for all aspects of the reaction dynamics at lower energies (the resonance region). However, this can be rectified by superimposing a number of s -channel resonance contributions in the Regge amplitude. This is the standard procedure,

that consists of identifying a small number of dominant resonances and replenishing these with a Regge background.

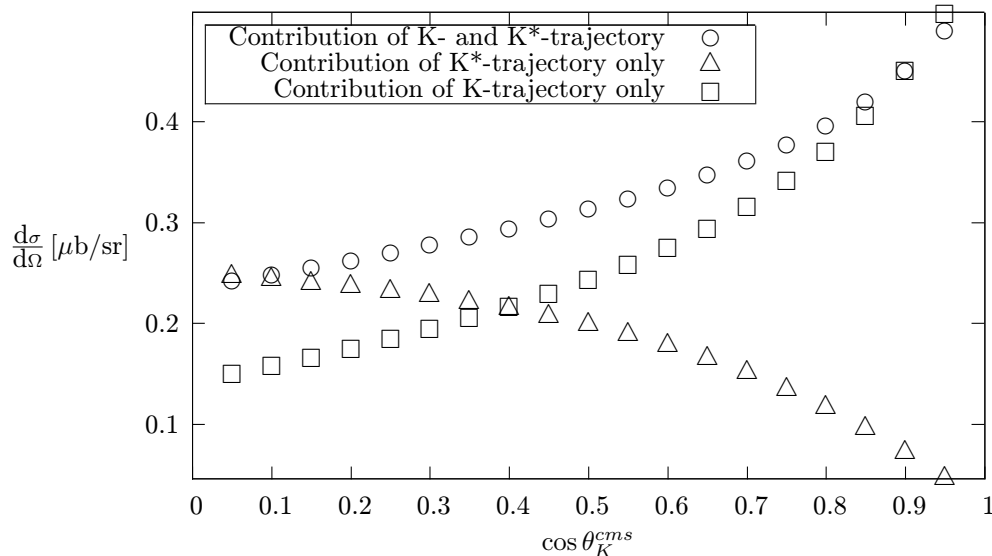


Figure 6.1: Contributions of K-trajectory and K*-trajectory to the total cross section in the center-of-mass frame in dependence of $\cos \theta_K^{cms}$ are shown (the photon energy in laboratory frame E_γ^{lab} is fixed at 1.3 GeV). As can be seen from the graph, the K*-trajectory is significant in the forward kaon angles, while the importance of K-trajectory grows with increasing kaon angle.

In practice, this means that from the isobar model program we leave out Born terms and all t - and u -channel contributions and refill them with the K- and K*-trajectories. This ensures the nonresonant background-shaped high-energy behaviour known from Regge model which describes the process for photon laboratory energy E_γ^{lab} up to 16 GeV. The resonant structure in lower energies is ensured by the resonant s -channel contributions we kept in the original program for isobar model. In the high-energy regime, $E_\gamma^{lab} \geq 4$ GeV, all the resonant contributions vanish due to including a Gaussian hadronic form factor (5.1) at $K\Lambda R$ vertices.

One question which could break this procedure is double counting. However, because the processes under study are largely background-dominated, the few added s -channel terms could be regarded as relatively small corrections, and double counting is not expected to pose a serious trouble.

Due to restoring the gauge invariance, the electric part of the s -channel Born term is attached to the kaon trajectory added to the original isobar model program.

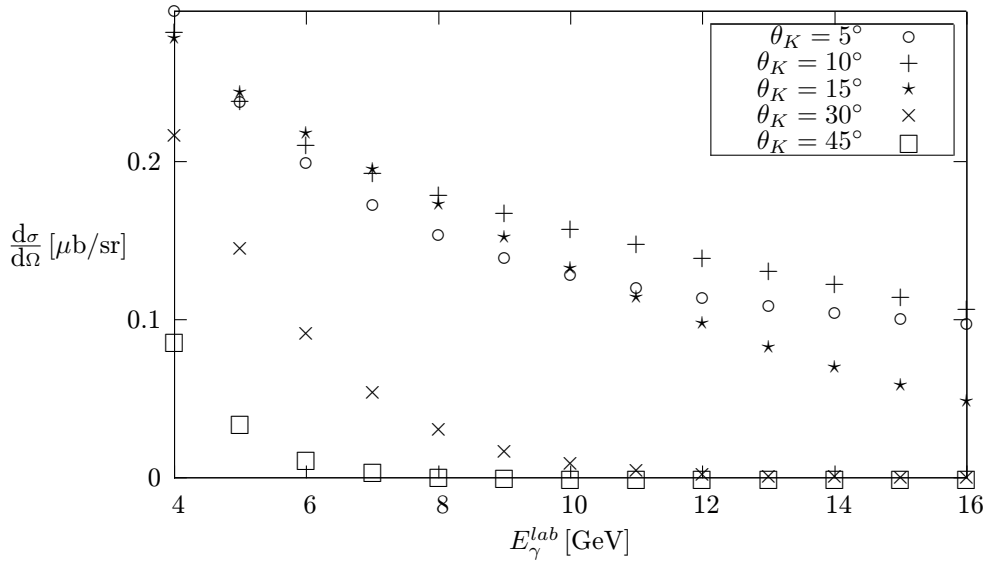


Figure 6.2: Cross section in the center-of-mass frame in dependence of the photon energy in the laboratory frame E_γ^{lab} for several kaon angles is shown. Range of E_γ^{lab} goes from 4 GeV to 16 GeV, therefore it is obvious, that these datapoints were calculated with the Regge model.

After the K^- - and K^* -trajectories were added to the isobar model, we had to do some tedious but necessary work. At first, it was needed to examine if both of the programs we were putting together have the same normalization of invariant amplitudes (and fortunately they have). After that, parameters of the kaon trajectories have to be added to the input as well as *e.g.* function

for the Gaussian hadronic form factor which is needed to ensure that the resonance amplitudes vanish at high values of E_γ^{lab} .

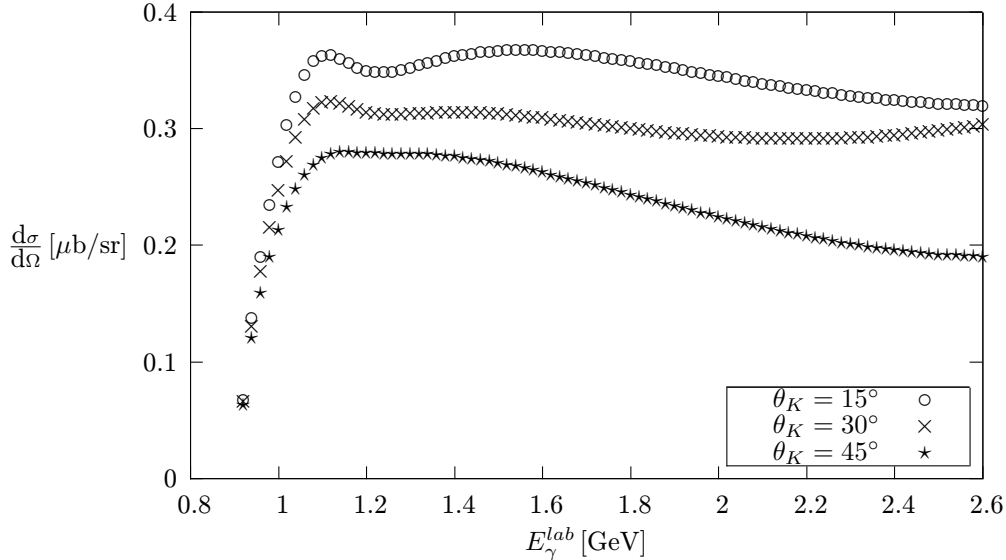


Figure 6.3: Cross section in the center-of-mass frame in dependence of the photon energy in the laboratory frame E_γ^{lab} for several kaon angles is shown. These datapoints were calculated with the original isobar model.

6.1 Discussion about the Outcomes

At first, it was necessary to compare the outcomes resulting from the new RPR-based program with graphs released in the articles. Firstly, the differential cross section for the reaction $\gamma + p \rightarrow K^+ + \Lambda$ for four photon energies $E_\gamma^{lab} = 5, 8, 11, 16$ GeV was calculated and the outcome was compared with Figure (18) in [13]. These two results appeared to be in perfect correspondence, as can be seen from the Figure (6.4). Therefore, it can be stated that the high-energy behaviour of the cross sections is with the new RPR-based program described very well.

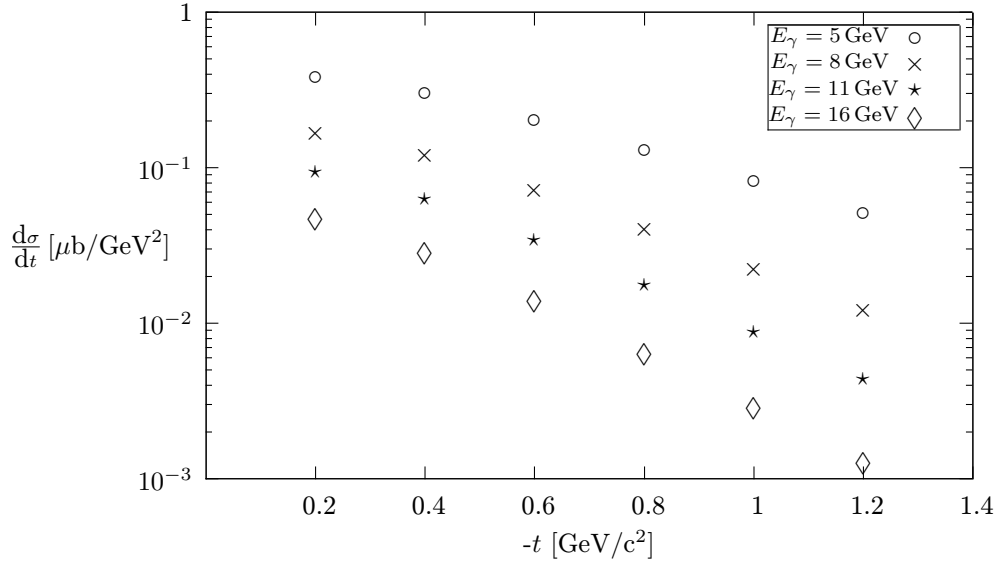


Figure 6.4: Differential cross section for the reaction $\gamma + p \rightarrow K^+ + \Lambda$ for four photon energies $E_\gamma^{lab} = 5, 8, 11, 16$ GeV. These datapoints were calculated with the RPR-based model.

In the resonance region it was necessary to tune parameters of the s -channel contributions. We did that by fitting to the low-energy data. Unfortunately, the value of χ^2 for the low-energy data is much bigger than one (it holds that the closer the value of χ^2 to one is, the better correspondence the model with experimental data gives).

As can be seen from comparison of Fig. (6.3) with Fig. (6.5), the cross sections calculated either with the original isobar model or with hybrid RPR model are of the same magnitude, but results from the RPR model overshoot results from the original isobar model. In addition, the expected resonance behaviour in the low-energy region is not obvious from the figure. This suggests that the parameters of the model still have to be tuned.

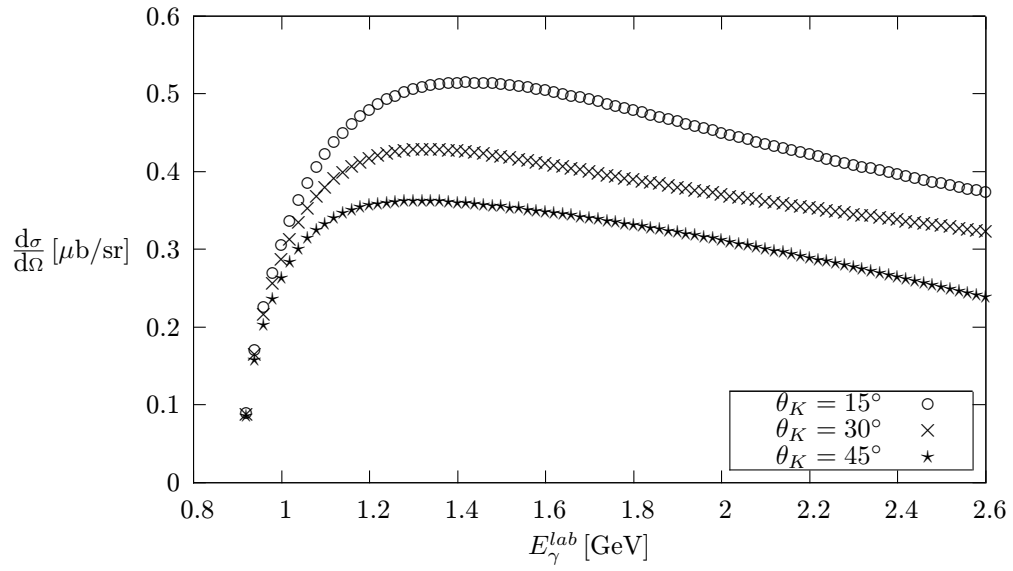


Figure 6.5: Cross section in the center-of-mass frame in dependence of the photon energy in the laboratory frame E_γ^{lab} for several kaon angles is shown. These datapoints were calculated with the hybrid RPR model.

Chapter 7

Conclusion

This thesis showed some of the basic properties of processes of photo- and electroproduction of kaons on nucleons. The study of these processes has rich history which goes back to the fifties, but there are still reasons, why these processes are important in contemporary physics.

There were sketched two main theoretical approaches for pseudoscalar meson photoproduction reactions - the isobar model and the Regge model. The latter provides good results at high energies and forward angles. Hereafter, the hybrid Regge-plus-resonance model, which is the approach of particular interest in this thesis, was outlined, too.

The main task of whole this research project was to build a program that can give reliable results. After a short description of the main theoretical approaches, there are showed several graphs resulting from that program. As can be seen from comparison *e.g.* with Ref. [13], the high-energy results are in a good agreement with the work of some other authors. What remains troublesome is the description of low-energy data. As it was stated before, the value of χ^2 for the low-energy data is too big. Improving the model and obtaining better correspondence between theoretical description and experimental data is a subject for further study.

Thanks to the importance of the photo- and electroproduction processes, the experimental community is interested in the search for missing resonances, which brings a flood of initiatives for the theoretical community. Many approaches to describe the photo- and electroproduction processes have been developed, but there is still room for questions and for the further analysis. While there is a very good description of photoproduction in forward angles which can be obtained with the RPR models, there is still room for some improvement. In future, it would be useful to extend the RPR amplitudes in backward angles, too.

Because of many of these unanswered questions, this topic could be very interesting for further research in the next years.

Appendix A

Isobar Model Formalism

A.1 CGLN Amplitudes

The relations between the CGLN amplitudes and the \mathcal{A}_j invariant functions are [9]

$$\mathcal{F}_1 = (\sqrt{s} - M_p)\mathcal{A}_1 - p_\gamma \cdot p_p \mathcal{A}_3 - p_\gamma \cdot p_\Lambda \mathcal{A}_4 - p_\gamma^2 \mathcal{A}_5,$$

$$\mathcal{F}_2 = \frac{|p_\gamma| \cdot |p_K|}{(E_p + M_p)(E_\Lambda + M_\Lambda)} [(\sqrt{s} - M_p)\mathcal{A}_1 - p_\gamma \cdot p_p \mathcal{A}_3 - p_\gamma \cdot p_\Lambda \mathcal{A}_4 - p_\gamma^2 \mathcal{A}_5],$$

$$\mathcal{F}_3 = \frac{|p_\gamma| \cdot |p_K|}{(E_p + M_p)} [-2p_\gamma \cdot p_p \mathcal{A}_2 + (\sqrt{s} + M_p)\mathcal{A}_4 + p_\gamma^2 \mathcal{A}_6],$$

$$\mathcal{F}_4 = \frac{|p_K|^2}{(E_\Lambda + M_\Lambda)} [2p_\gamma \cdot p_p \mathcal{A}_2 (\sqrt{s} - M_p)\mathcal{A}_4 - p_\gamma^2 \mathcal{A}_6],$$

$$\mathcal{F}_5 = \frac{|p_\gamma|^2}{(E_p + M_p)} [-\mathcal{A}_1 + 2p_\gamma \cdot p_\Lambda \mathcal{A}_2 + (\sqrt{s} + M_p)(\mathcal{A}_3 - \mathcal{A}_5) + p_\gamma \cdot p_\Lambda \mathcal{A}_6]$$

$$\begin{aligned} \mathcal{F}_6 = & \frac{|p_\gamma| \cdot |p_K|}{(E_\Lambda + M_\Lambda)} [-2p_\gamma \cdot p_\Lambda \mathcal{A}_2 + (\sqrt{s} - M_p)\mathcal{A}_3 - p_\gamma \cdot p_\Lambda \mathcal{A}_6 \\ & - \frac{1}{E_p + M_p} (p_{\gamma 0} \mathcal{A}_1 + p_\gamma \cdot p_p \mathcal{A}_3 + p_\gamma \cdot p_\Lambda \mathcal{A}_4 + p_{\gamma 0} (\sqrt{s} + M_p)\mathcal{A}_5)], \end{aligned}$$

Bibliography

- [1] A. Bleckmann, S. Herda, U. Opara, W. Schulz, W. J. Schwille, and H. Urbahn, *Z.Phys.* 239, 1 (1970)
- [2] R. Bradford *et al.*, *Phys.Rev. C* 73, 035202 (2006)
- [3] R. Bradford *et al.*, *Phys. Rev. C* 75, 035205 (2007)
- [4] P. Bydzovsky *et al.*, arXiv:nucl-th/0305039v1 (2003)
- [5] W.-T. Chiang, F. Tabakin, T.-S. H. Lee, and B. Saghai, *Phys. Lett. B* 517, 101 (2001)
- [6] T. Corthals, *Regge-plus-resonance Approach to Kaon Production from the Proton*, PhD Thesis, Gent University, 2006-2007
- [7] T. Corthals *et al.*, In Proc. of *The 11th Workshop on the Physics of Excited Nucleons*, edited by H. Hammer, V. Kleber, U. Thoma and H. Schmieden (Springer Berlin Heidelberg, 2008), page 247
- [8] T. Corthals *et al.*, In Proc. of *The IX International Conference on Hypernuclear and Strange Particle Physics*, edited by J. Pochodzalla, T. Walcher (Springer Berlin Heidelberg, 2007), page 350
- [9] J.C. David, C. Fayard, G. H. Lamot and B. Saghai, *Phys. Rev. C* 53, 2613 (1996)

- [10] P. L. Donoho and R. L. Walker, Phys. Rev. 107, 1198 (1957)
- [11] T. Fujii *et al.*, Phys. Rev. D 2, 439 (1970)
- [12] K.-H. Glander *et al.*, Eur. Phys. J. A 19, 251 (2004)
- [13] M. Guidal, J.-M. Laget, and M. Vanderhaeghen, Nucl. Phys. A 627, 645 (1997)
- [14] S. Janssen, J. Ryckebusch, D. Debruyne, T. Van Cauteren, Phys. Rev. C 66, 035202 (2002)
- [15] T. K. Kuo, Phys. Rev. 129, 2264 (1963)
- [16] R. Lawall *et al.*, Eur. Phys. J. A 24, 275 (2005)
- [17] A. Lleres *et al.*, Eur. Phys. J. A 31, 79 (2007)
- [18] J. W. C. McNabb *et al.*, Phys. Rev. C 69, 042201(R) (2004)
- [19] A. Silverman, R. R. Wilson, and W. M. Woodward, Phys. Rev. 108, 501 (1957)
- [20] D. Skoupil, *Electroproduction of Kaons on Nucleons*, Bachelor Thesis, CTU Prague, 2009-2010
- [21] M. Sumihama *et al.*, Phys. Rev. C 73, 035214 (2006)
- [22] M. Q. Tran *et al.*, Phys. Lett. B 445, 20 (1998).
- [23] H. Thom, Phys. Rev. 151, 1322 (1966)
- [24] R. G. T. Zegers *et al.*, Phys. Rev. Lett. 91, 092001 (2003)